JOURNAL OF SOLID STATE CHEMISTRY **125,** 125–132 (1996)
ARTICLE NO. 0274

A HREM Study on $La_{1/3}Sr_{2/3}FeO_{3-y}$ II. ($0.15 \leq y \leq 0.33$)

E. García-González,* M. Parras,* J. M. González-Calbet,*,[1] and M. Vallet-Regí†

*Departamento de Química Inorgánica, Facultad de Químicas, Universidad Complutense, 28040 Madrid, Spain; and
†Departamento de Química Inorgánica y Bioinorgánica, Facultad de Farmacia, Universidad Complutense, 28040 Madrid, Spain

Received December 28, 1995; in revised form April 26, 1996; accepted May 2, 1996

The microstructural characterization of $La_{1/3}Sr_{2/3}FeO_{3-y}$ ($y = 0.15$ and $y = 0.33$) materials has been studied by means of electron diffraction and high-resolution electron microscopy. A new unit cell of parameters $2a_c\sqrt{2} \times 3a_c \times \sqrt{2}_c$ has been observed for the highly reduced material $La_{1/3}Sr_{2/3}FeO_{2.67}$ (or $LaSr_2Fe_3O_8$) as a consequence of the anionic vacancy order. This cell seems to avoid any ordered distribution of Sr and La in the *A* sublattice, which is only possible for a random distribution of oxygen vacancies ($y = 0.15$).

INTRODUCTION

Much work has been devoted to $AFeO_{3-y}$ perovskite-like materials, in which the anionic vacancy distribution and the final symmetry of the phases are strongly influenced by the *A* cations. In such oxygen-deficient phases, the stabilization energy of the different oxygen polyhedra found in dependence of the accommodated *B* cations has not been quantified but is obviously important for the type of structural framework.

In the *RE*–Ba–Cu–O (*RE* = rare earth) system, the 1:2:3 ratio has been the most widely studied. The different anionic coordinations that can be adopted by the copper atoms have allowed several oxygen-deficient perovskites (1, 2). Full replacement of Cu by Co has been achieved, the resulting compound having two Co atoms in square pyramidal coordination and one Co atom octahedrally coordinated (3). When copper is substituted by iron maintaining the 1:2:3 ratio, the differences in stability at the metallic sites lead to other results in the *RE*–Ba–Fe–O system. In a previous paper (4), we reported that Dy(Ho) $Ba_2Fe_3O_8$ can also be described as a threefold perovskite superstructure, the stacking sequence being ... *POP* ... (*P*, square pyramid; *O*, octahedron) isostructural with $YBa_2Fe_3O_8$ (5).

In the $LaFeO_3$–$Ca_2Fe_2O_5$ perovskite-related system, compositional variations lead to the $LaCa_2Fe_3O_8$ ordered phase (1:2:3), where two octahedral layers alternate with a tetrahedral layer along the *b* axis, the stacking sequence being ... *OOT* ... (*T*, tetrahedron) (6), which in the following we will call the *G* phase. This is the only ordered phase isolated for the cationic ratio 1:2:3, La:Ca:Fe. Anionic compositions higher than O_8 led to microdomain formation (7). Most of the rare earth elements lead to the *G* phase in the Ca system (8). When Ca is replaced by Ba in the above 1:2:3 phase, two different situations can occur depending on the Fe(IV) content. When the material contains 38% Fe(IV), a simple cubic phase is obtained (9); however, when all iron is in the three oxidation state ($La_{1/3}Ba_{2/3}FeO_{2.67}$//$LaBa_2Fe_3O_8$), the material appears to consist of three-dimensional microdomains (10).

The occurrence of the *OOT* sequence in $LaCa_2Fe_3O_8$ has been verified by TEM (7); a similar *OOT* stacking sequence in the Ca–Fe–Mn–O and Ca–Fe–Ti–O systems has been reported (11, 12) and a partial structural refinement was obtained from X-ray powder diffraction data. When Ca is replaced by Sr, only the presence of La, among the *RE* elements, gives rise to the layer sequence ... *OOT* ... (6, 13). By increasing the oxygen content in the material, thus leading to the $O_{8.5}$ composition, Battle *et al.* (14) formulated an intuitive structural model on the basis of layers of Fe^{4+} in five-coordinated sites, separated by two layers of Fe^{3+} in octahedral sites.

The study of the accommodation of compositional variations in the $La_{1/3}Sr_{2/3}FeO_{3-y}$ system has shown (15) that for the $y = 0.1$ composition, La and Sr are ordered in small domains preserving the 1:2 ratio and following a sinusoidal modulation. Continuing this microstructural study, we report here the results concerning the microstructural aspects of $La_{1/3}Sr_{2/3}FeO_{3-y}$ for $y = 0.15$ and $y = 0.33$. The electron diffraction and microscopy investigation has led to a better understanding of the crystal chemistry of the $La_{1/3}Sr_{2/3}FeO_{3-y}$ phases.

EXPERIMENTAL

Stoichiometric amounts of $SrCO_3$, La_2O_3, and α-Fe_2O_3 of AnnalaR quality were mixed and heated at 1300°C for

[1] To whom correspondence should be addressed.

0022-4596/96 $18.00

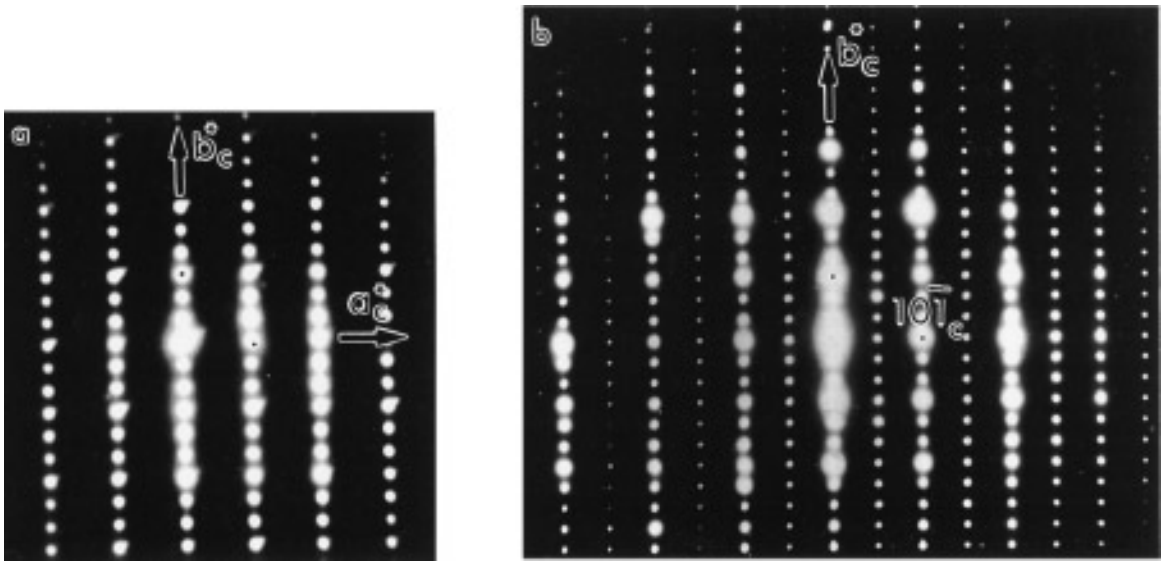

FIG. 1. SAED patterns corresponding to $La_{1/3}Sr_{2/3}FeO_{2.67}$ along (a) $[001]_c$ and (b) $[101]_c$ zone axes.

96 h in air to achieve the $La_{1/3}Sr_{2/3}FeO_{2.90}$ composition. Aliquots of this material were then treated in two different ways:

—Aliquots were annealed in argon for 36 h at 1150°C before they were slow cooled in Ar to room temperature; after such treatment the $La_{1/3}Sr_{2/3}FeO_{2.85}$ composition was obtained, as determined by thermogravimetric analysis on a CAHN D-200 electrobalance.

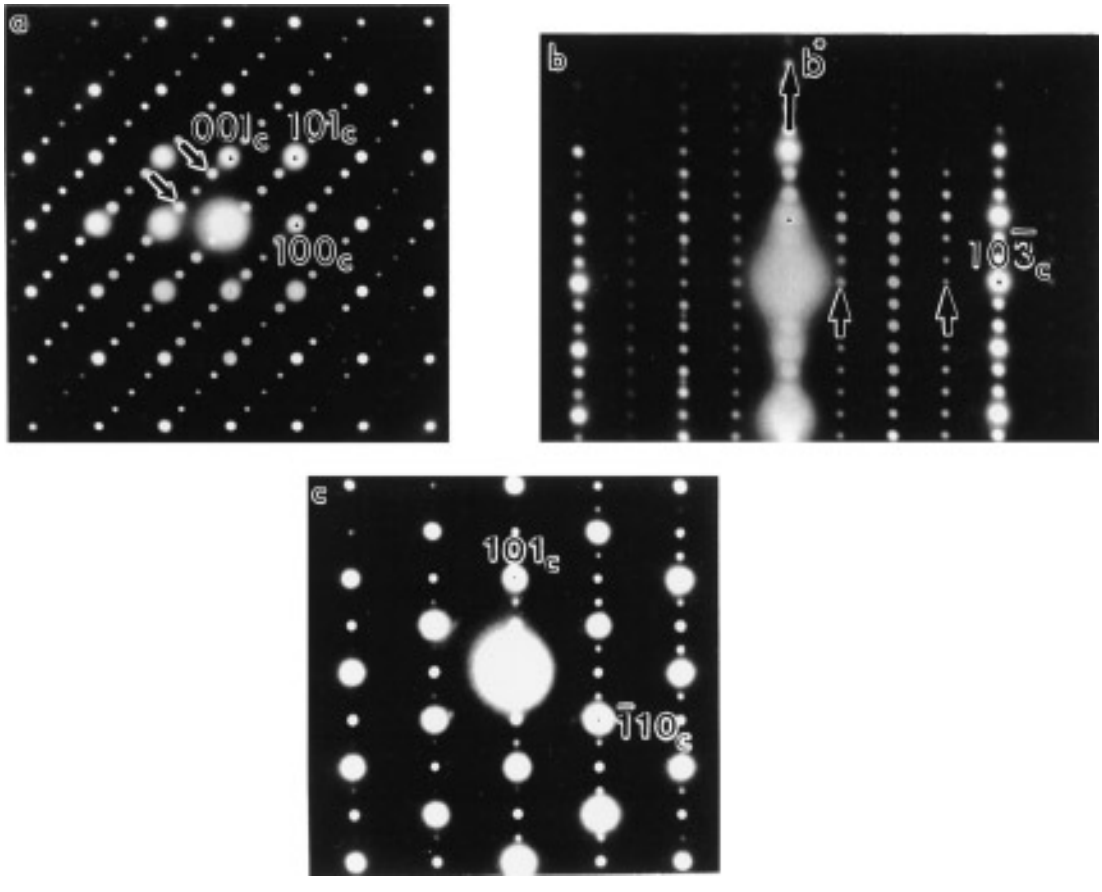

FIG. 2. SAED patterns for $La_{1/3}Sr_{2/3}FeO_{2.67}$ along (a) $[010]_c$, (b) $[301]_c$, and (c) $[\bar{1}\bar{1}1]_c$ zone axes. Arrows in the patterns indicate extra spots with respect to the *G* phase.

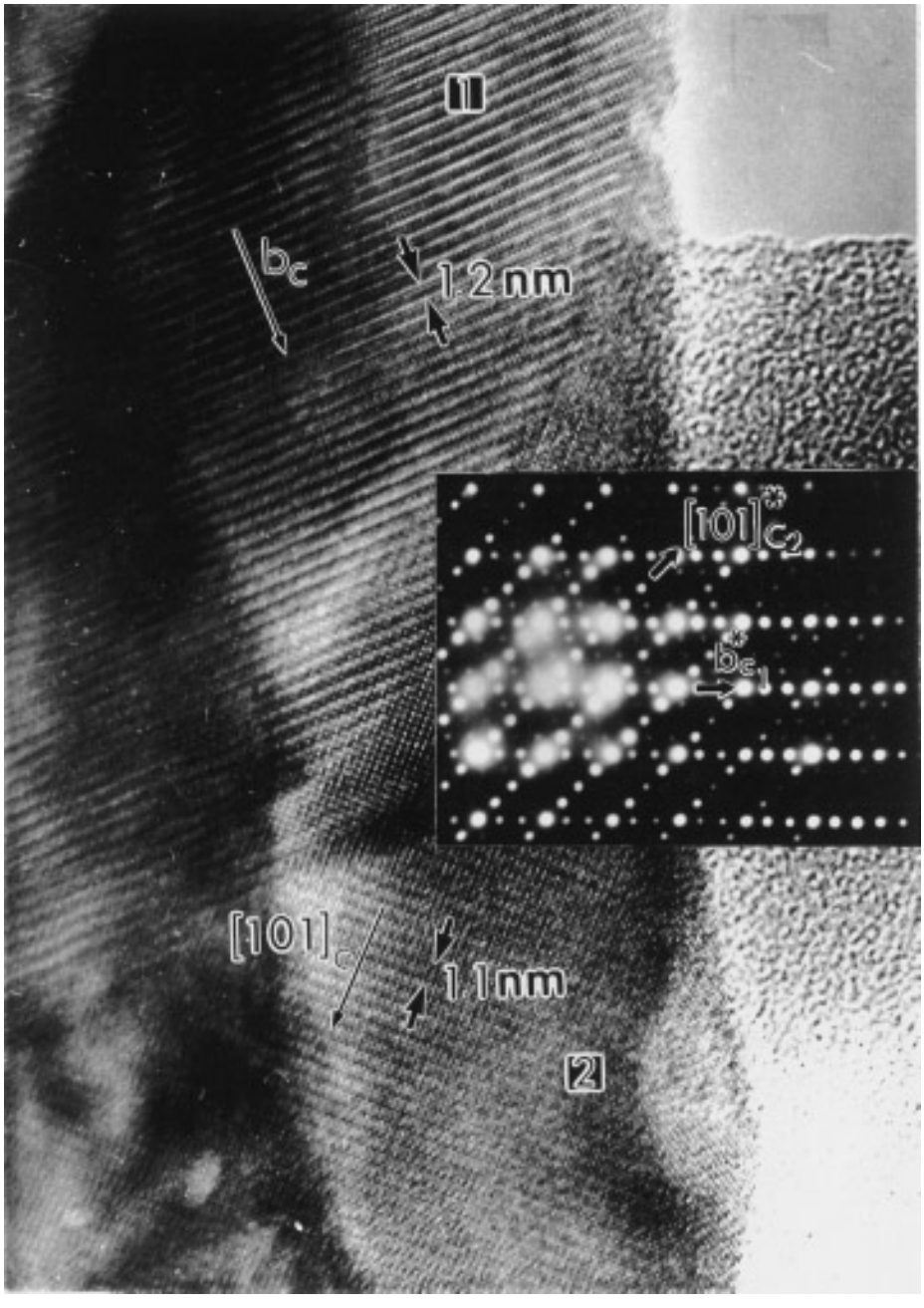

FIG. 3. High-resolution electron micrograph for $La_{1/3}Sr_{2/3}FeO_{2.67}$. Domains 1 and 2 correspond to the $[001]_c$ and $[010]_c$ projections, respectively. The corresponding SAED pattern is shown in the inset.

—Aliquots were annealed in 10% H_2/Ar at 300°C for 12 h before they were cooled to room temperature in the reducing atmosphere; the homogeneous brown product obtained corresponded to $La_{1/3}Sr_{2/3}FeO_{2.67}$. The oxygen content was established as stated above.

The oxidation state of iron was also determined by titration after dilution in 3 *N* HCl with an excess of Mohr salt. The average cationic composition was determined by inductive coupling plasma (ICP). In both cases, the average value obtained closely coincides with the nominal composition.

Powder X-ray diffraction (XRD) was performed on a Siemens D-5000 diffractometer with a graphite monochromator and using Cu$K\alpha$ radiation.

The samples for electron microscopy were ultrasonicaly dispersed in *n*-butanol and transferred to carbon-coated copper grids. Selected area electron diffraction (SAED) was carried out on a JEOL 2000FX electron microscope.

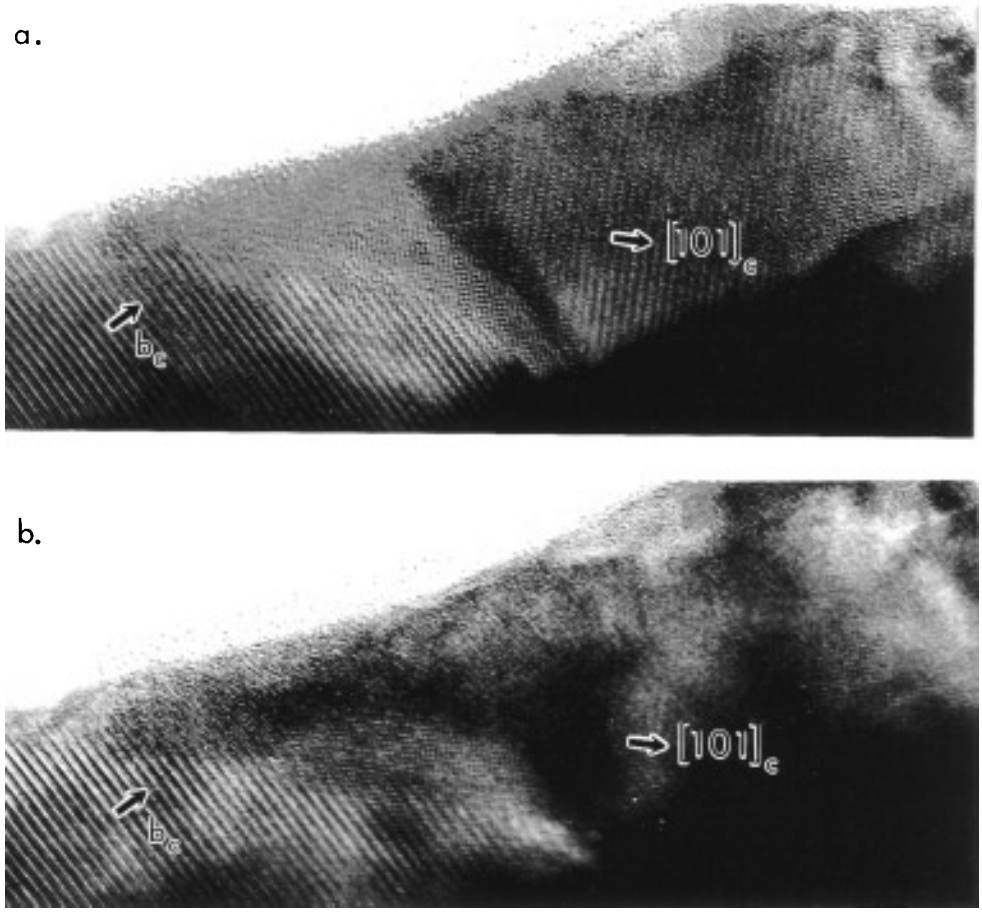

FIG. 4. (a and b) High-resolution electron micrographs for $La_{1/3}Sr_{2/3}FeO_{2.67}$ taken with a difference of 50 s to show the vanishing of the fourfold superstructure with electron beam irradiation.

High-resolution electron microscopy (HREM) was performed on a JEOL 4000EX electron microscope.

RESULTS AND DISCUSSION

$La_{1/3}Sr_{2/3}FeO_{2.67}$ ($= LaSr_2Fe_3O_8$)

The annealing of the $O_{2.90}$ sample in reducing atmosphere, as previously detailed, gives rise to a material with all iron in the (III) oxidation state, that is, the $La_{1/3}Sr_{2/3}FeO_{2.67}$ composition. From XRD, an orthorhombic distortion of the simple cubic subcell is clearly appreciated. The maxima can be indexed on the basis of an orthorhombic unit cell (6) related to the cubic perovskite subcell by $a_c\sqrt{2} \times 3a_c \times a_c\sqrt{2}$ in agreement with the structural refinement reported by Battle *et al.* (13) on a sample with the same nominal composition.[2] Figures 1a and 1b correspond to the SAED patterns of this material along the $[001]_c$ and $[101]_c$ zone axes. Effectively, these patterns can be assigned as reciprocal planes of the well known *G* phase. At this point, it is important to mention that the occurrence of the threefold superstructure along b_c in this phase has been attributed to anionic vacancy ordering and no evidence for La/Ca associated order has been found.

When tilting around a_c^* from the $[001]_c$ projection, the $[010]_c$ zone axis (Fig. 2a) shows two extra spots marked

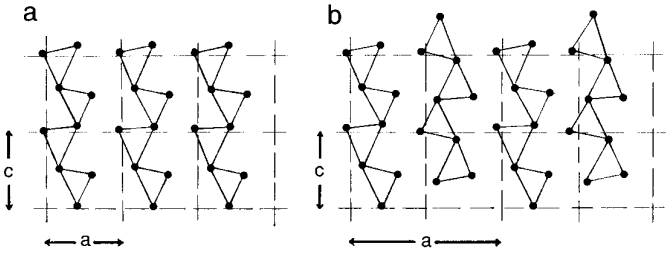

FIG. 5. (a) Schematic representation of the tetrahedral layers for the *G* and *B* structures seen along the [010] ($[101]_c$) direction. Only oxygen atoms are represented for simplicity. (b) Hypothetical distribution of the tetrahedral rows in the tetrahedral layers for $La_{1/3}Sr_{2/3}FeO_{2.67}$.

[2] Subindex c refers to the basic perovskite subcell.

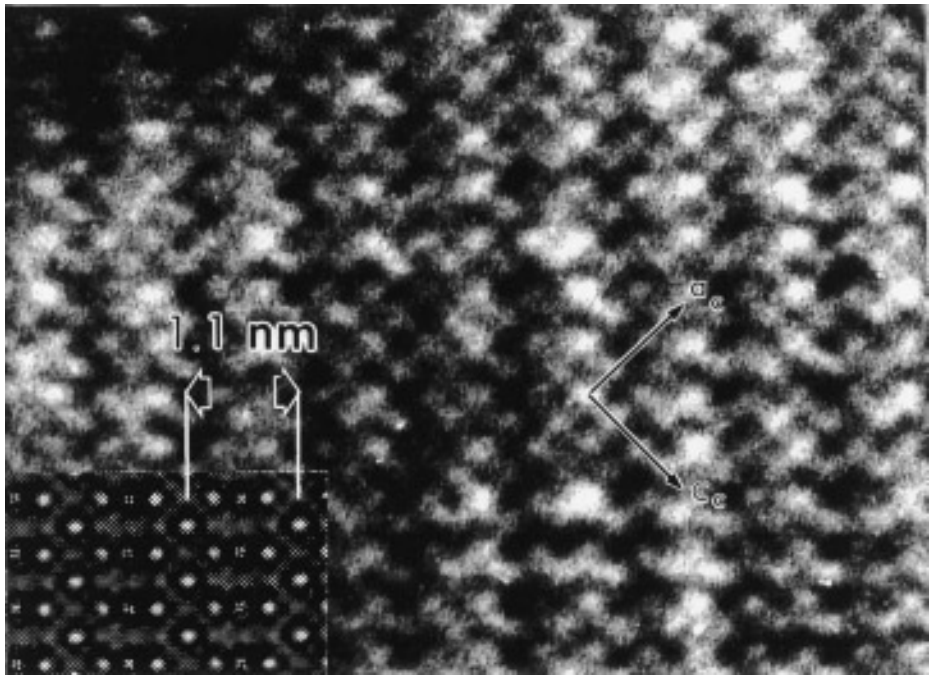

FIG. 6. HREM image for $La_{1/3}Sr_{2/3}FeO_{2.67}$ along the [010] zone axis. The simulated image is shown in the inset.

with arrows, with respect to the *G* phase along $[101]_c$*, i.e., a fourfold superstructure along this direction. This feature can also be observed in the $[301]_c$ zone axis (Fig. 2b), where two extra rows of spots are seen at $(1/4\ k\ 3/4)_c$ and $(3/4\ k\ 9/4)_c$. Figure 2c corresponds to the $[\bar{1}\bar{1}1]_c$ projection, where the fourfold superstructure is clearly seen along $[101]_c$.

From the above results, a new cell of parameters $a_c\sqrt{2} \times 3a_c \times a_c\sqrt{2}$ can be proposed; that is, the *a* axis is doubled with respect to the *G* phase. The image in Fig. 3 corresponds to the HREM micrograph of one crystal of $La_{1/3}Sr_{2/3}FeO_{2.67}$. Two domains intergrown at 45° are visible: number 1 corresponds to the $[001]_c$ zone axis and number 2 to the $[010]_c$ projection. The inset shows the corresponding SAED pattern.

According to the oxygen composition determined by chemical and thermogravimetrical analysis, and taking into account the ability of iron to adopt tetrahedral, square pyramidal, and octahedral coordination, three vacancy distributions would lead to a threefold superstructure:

—a sequence constituted by two octahedral layers and one tetrahedral layer alternating along the $[010]_c$ direction, like in the *G* phase,

—a stacking sequence formed by two square pyramidal layers and one octahedral layer along the $[010]_c$ direction (... *POP* ...), where the square base of the pyramids is parallel to the b_c axis, like the $Ca_2Mn_2O_5$ (16), and

—the last sequence (... *POP* ...) with the square base of the pyramids perpendicular to the b_c axis.

These situations are able to produce a threefold superlattice of the perovskite structure, and they are also compatible with the existence of order between La and Sr cations. The last polyhedra arrangement would give rise to a unit cell of parameters $a_c \times 3a_c \times a_c$ (4), which is not in agreement with the reciprocal lattice obtained by SAED.

In the second distribution ... *POP* ..., the vacancy order in two of every three (010) BO_2 planes of cubic perovskite with alternate $[101]_c$ strings of oxygen atoms that are missing every other oxygen would lead to the $2a_c\sqrt{2} \times 3a_c \times a_c\sqrt{2}$ periodicity. Then if the ... *OOT* ... sequence along b_c is preserved, the fourfold superstructure observed must be caused by a structural modification that does not imply any change in composition.

To continue the discussion, it is worth mentioning that this superstructure tends to disappear under electron beam irradiation, although the transformation is relatively slow (see Figs. 4a and 4b). According to this fact, the structural change can be imagined as a consequence of a rearrangement in the oxygen sublattice, since the oxygen atoms are the lightest.

Figure 5a is a schematic drawing of the tetrahedral layers of the *G* and *B* (brownmillerite (17)) structures seen along the [010] direction. The tetrahedral layers in the *G* structure all have the same orientation, while in the *B* structure they are related by a rotation of 180° along the *b* axis. The figure shows the tilt of the tetrahedra when the oxygen rows along the $[101]_c$ direction are empty. The *G*-type material can be obtained either with two different cations occupying the *A* positions of the perovskite substructure, as in $LaCa_2Fe_3O_8$, or with two cations in the *M* sites, as

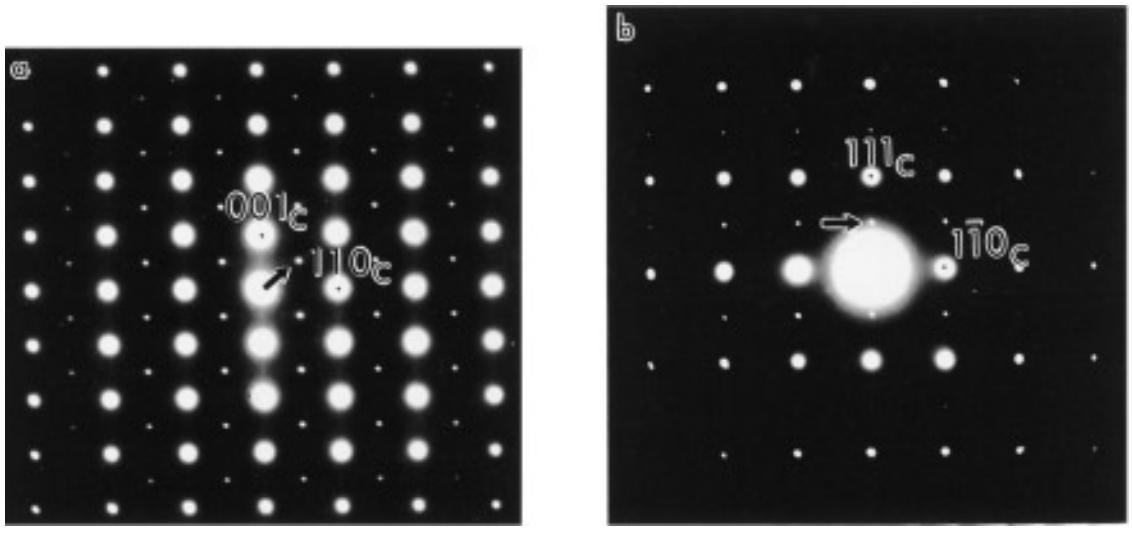

FIG. 7. SAED patterns for $La_{1/3}Sr_{2/3}FeO_{2.85}$ along the (a) $[1\bar{1}0]_c$ and (b) $[11\bar{2}]_c$ zone axes.

in $Ca_3Fe_2TiO_8$ (12). Since no detailed crystal structure is available for $LaCa_2Fe_3O_8$, data from the structural refinement of $Ca_3Fe_2TiO_8$ have been used in Fig. 4. There are no major differences between the *M* coordination polyhedra of the *G* and *B* structures.

If we imagine now that one of every two of the tetrahedra rows inside a tetrahedral layer is tilted 180° around [010], the arrangement drawn in Fig. 5b is achieved, and thus doubling of the *a* axis occurs. This operation would imply only the movement of some oxygen atoms and would not affect either the *c* or the *b* axis. This tetrahedra disposition was previously postulated by Harder and Müller-Buschbaum (18) when studying by X-ray single crystal methods $Sr_2Fe_2O_5$ in comparison with other $A_2B_2O_5$ compounds. The occurrence of such a structural rearrangement would be in agreement with the results obtained by SAED.

Lets consider now the ... *POP* ... distribution we mentioned before to be responsible for the found periodicity. Its disappearance under electron beam irradiation would imply, given the structural refinement reported by Battle *et al.* (13) and taking into account that all iron is in the three oxidation state, a change in the iron(III) coordination environment in two of the three layers, changing the sequence from ... *POPPOP* ... to ...*OOTOOT* .... Such a change should be distinguishable also along the *b* axis of the structure, i.e., along the layer stacking direction. However, the contrast remains unchanged along *b* during the transformation, as can be observed in Fig. 4.

Therefore, it seems reasonable to think of the ... *OOT* ... sequence of the *G* phase as being preserved in the material under discussion.

In order to confirm this structural model, image simulation has been carried out (19) using as input data the atomic coordinates generated from the atomic parameters in Ref. (13) for $LaSr_2Fe_3O_8$ and without any restriction in symmetry (S.G. *P*1). The corresponding calculated image has been included as an inset in Fig. 6 (the agreement between the experimental and calculated images is satisfactory for $\Delta f = -70$ nm and $t = 6.0$ nm). As can be observed, the change in contrast along $[100]_c$ leads to doubling of the a_G axis, in agreement with the experimental image. Differences in contrast are not appreciable when Sr and La are ordered or are not ordered in the *A* sublattice. Therefore, a random distribution for the *A* atoms has been considered in the input data.

At this point, it is worth recalling that a similar transformation without composition change has been found to occur in $Sr_2Co_2O_5$ (20) in a reversible way as a function of irradiation time under the electron beam.

Further structural analysis by means of neutron diffraction is in progress to confirm the structural features presented.

$La_{1/3}Sr_{2/3}FeO_{2.85}$ (= $LaSr_2Fe_3O_{8.55}$)

As previously mentioned, this sample was obtained from the $O_{2.90}$ composition by controlled reduction under Ar. The XRD pattern showed only reflections corresponding to a pseudocubic perovskite-type unit cell. However, the electron microscopy study indicated that this sample was more complex.

From the electron diffraction study, no extra feature with respect to the cubic subcell is observed along the $[001]_c$ and $[1\bar{1}1]_c$ zone axes. However, by tilting 45° around a_c^* (Fig. 7a) an extra reflection is observed, doubling the $[111]_c$ direction. This feature is also observed in the $[11\bar{2}]_c$

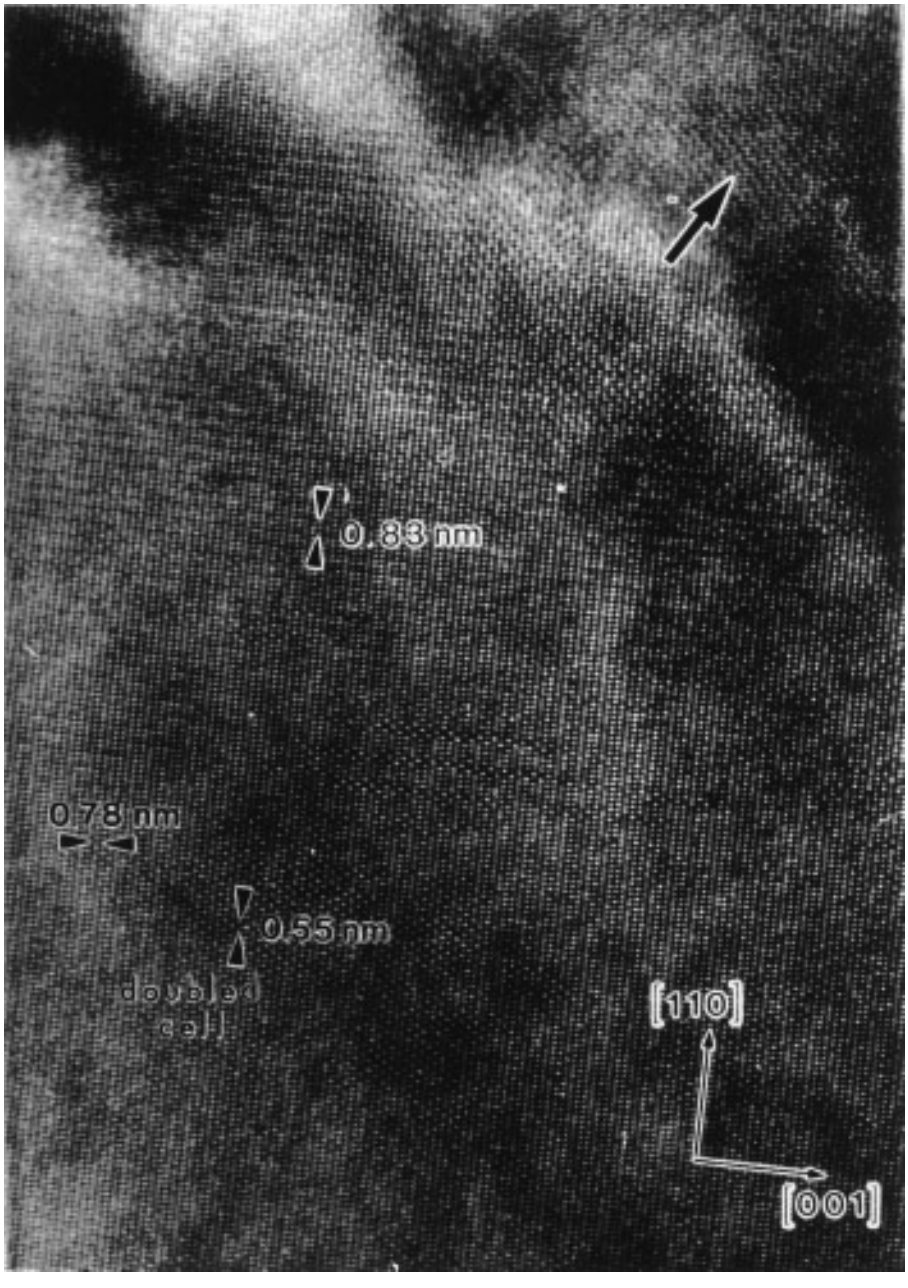

FIG. 8. HREM image for $La_{1/3}Sr_{2/3}FeO_{2.85}$ taken along the $[1\bar{1}0]_c$ zone axis.

zone axis (Fig. 7b). The fact that this extra reflection is observed only with SAED and not with XRD indicates that the material has a cubic unit cell of parameter $2a_c$ only in some domains inside the crystals. A similar situation has been already observed in the La–Ba–Fe–O system (9). Figure 8 corresponds to the HREM image taken along the $[1\bar{1}0]_c$ zone axis. Effectively, areas with double contrast along the two orthogonal directions are observed and are responsible for the double unit cell found by electron diffraction. Small regions are still visible, as previously stated for the $O_{2.90}$ composition (15), where La and Sr must be ordered, preserving the 1:2 ratio (see the zone marked with the arrow). In this sense, some areas remain where a triple contrast along $[110]_c$ is observed and others where $[001]_c$ is doubled. These domains are responsible for the diffuse diffraction maxima observed at $(1/31/31/2)_c$ and $(2/32/31/2)_c$ and at $(001/2)_c$ (see Fig. 7a).

An ordered distribution of oxygen vacancies and/or La–Sr atoms in the *A* sublattice could be responsible for the doubling of the unit cell. Taking into account the average anionic composition of this sample, the most favorable oxygen vacancy distribution would lead to the ... *OPOP*

... sequence in the doubled cell areas. A similar structural discussion on the basis of Mössbauer spectroscopy data has been reported by Battle *et al.* (14). This arrangement corresponds to the $O_{2.75}$ local composition, which would imply the existence of fully oxidized ($O_{3.00}$) domains to reach the average value. Provided that the material has been obtained after it was annealed in reducing atmosphere, the presence of such oxygen-rich areas seems quite improbable (15).

Therefore, the most suitable origin of the double perovskite cell areas is related to strontium–lanthanum ordering in the *A* positions in such a way that a lanthanum atom has strontium as closest *A* neighbors and a strontium atom is surrounded by lanthanum atoms. Since the nominal composition implies a 2:1 Sr:La ratio, some domains must exist where La is in defect, and some others where a random distribution of the *A* cations takes place.

Our first studies in the $La_{1/3}Sr_{2/3}FeO_{3-y}$ system (15) have shown the appearance of partial cationic order for the $y = 0.1$ composition and the vanishing of this short range order situation when no oxygen vacancies are present. For the highest reduced composition investigated, $y = 0.33$, the anionic vacancy order leading to a unit cell of parameters $2a_c\sqrt{2} \times 3a_c \times a_c\sqrt{2}$ seems to avoid an ordered arrangement in the *A* sublattice; a 1:1 Sr:La order takes place during partially oxidization up to the $y = 0.15$ composition. Thus, it can be concluded that ordering in the *A* sublattice seems to occur only when the oxygen vacancies are randomly distributed, which is reasonable considering the similar ionic radii of both cations.

ACKNOWLEDGMENTS

We acknowledge the financial support of CICYT (Spain) through Research Projects MAT93-0207 and MAT95-0642. We are also grateful to the Centro de Microscopía Electrónica (UCM) for facilities, and especially to E. Baldonedo for valuable technical assistance.

REFERENCES

1. J. J. Capponi, C. Chaillout, A. W. Hewat, P. Lejay, M. Marezio, N. Nguyen, B. Raveau, J. L. Soubeyroux, J. L. Tholence, and R. Tournier, *Europhys. Lett.* **3,** 1301 (1987).
2. P. Bordet, C. Chaillout, J. J. Capponi, J. Chenavas, and M. Marezio, *Nature* **327,** 306 (1987).
3. S. Geremia, G. Nardin, R. Mosca, L. Randaccio, and E. Zangrando, *Solid State Commun.* **72,** 333 (1989).
4. E. García-González, M. Parras, J. M. González-Calbet, and M. Vallet-Regí, *J. Solid State Chem.* **104,** 232 (1993).
5. Q. Huang, P. Karen, V. L. Karen, A. Kjekshus, J. W. Lynn, A. D. Mighell, N. Rosov, and A. Santoro, *Phys. Rev. B* **45**(17), 9611 (1992).
6. J. C. Grenier, M. Pouchard, and P. Hagenmuller, *Struct. Bonding* **47,** 1 (1981).
7. M. A. Alario-Franco, M. J. R. Henche, M. Vallet, J. M. G. Calbet, J. C. Grenier, A. Wattiaux, and P. Hagenmuller, *J. Solid State Chem.* **46,** 23 (1983).
8. M. A. Sekina, J. P. Bonnet, J. C. Grenier, M. Onillon, M. Pouchard, and P. Hagenmuller, *Rev. Chim. Miner.* **17,** 431 (1980).
9. M. Parras, M. Vallet-Regí, J. M. González-Calbet, M. A. Alario-Franco, and J. C. Grenier, *J. Solid State Chem.* **74,** 110 (1988).
10. J. M. González-Calbet, M. Parras, M. Vallet-Regí, and J. C. Grenier, *J. Solid State Chem.* **92,** 110 (1991).
11. N. Nguyen, Y. Calage, F. Vanet, G. Ferey, V. Caignaert, M. Hervieu, and B. Raveau, *J. Solid State Chem.* **53,** 398 (1984).
12. J. Rodríguez-Carvajal, M. Vallet-Regí, and J. M. González-Calbet, *Mater. Res. Bull.* **24,** 423 (1989).
13. P. D. Battle, T. C. Gibb, and P. Lightfoot, *J. Solid State Chem.* **84,** 237 (1990).
14. P. D. Battle, T. C. Gibb, and S. Nixon, *J. Solid State Chem.* **79,** 75 (1989).
15. E. García-González, M. Parras, J. M. González-Calbet, and M. Vallet-Regí, *J. Solid State Chem*., in press.
16. K. R. Poeppelmeir, M. E. Leonowicz, J. C. Scanlon, J. M. Longo, and W. B. Yelon, *J. Solid State Chem.* **45,** 71 (1982).
17. E. F. Bertaut, L. Blum, and A. Sagnieres, *Acta Crystallogr.* **12,** 149 (1959).
18. M. Harder and H. K. Müller-Buschbaum, *Z. Anorg. Allg. Chem.* **464,** 169 (1980).
19. "NCEMSS Programm." National Center for Electron Microscopy, Material and Chemical Science Division, Laurence Berkeley Laboratory, University of California.
20. J. M. González-Calbet and J. Rodríguez, "Inst. Phys. Conf. Ser. 93," Vol. 2, Chap. 10. 1988.